Title

Analytical harmonic vibrational frequencies with VV10-containing density functionals: Theory, efficient implementation, and benchmark assessments

Journal

The Journal of Chemical Physics, 158(20)

ISSN

0021-9606

Authors

Liang, Jiashu

Feng, Xintian

Liu, Xiao

et al.

Publication Date

2023-05-28

DOI

10.1063/5.0152838

Analytical harmonic vibrational frequencies with VV10-containing density functionals: Theory, efficient implementation, and benchmark assessments.

Jiashu Liang,[1] Xintian Feng,[2] Xiao Liu,[1] and Martin Head-Gordon[1,3]

[1)]*Kenneth S. Pitzer Center for Theoretical Chemistry, Department of Chemistry, University of California at Berkeley, Berkeley, CA 94720, USA*

[2)]*Q-Chem Inc., Pleasanton, CA 94588, USA*

[3)]*Chemical Sciences Division, Lawrence Berkeley National Laboratory, Berkeley, CA 94720, USA*

(*Electronic mail: mhg@cchem.berkeley.edu)

(Dated: 1 June 2023)

VV10 is a powerful nonlocal density functional for long-range correlation that is used to include dispersion effects in many modern density functionals such as the meta-generalized gradient approximation (mGGA), B97M-V, the hybrid GGA, ωB97X-V and the hybrid mGGA, ωB97M-V. While energies and analytical gradients for VV10 are already widely available, this study reports the first derivation and efficient implementation of the analytical second derivatives of the VV10 energy. The additional compute cost of the VV10 contributions to analytical frequencies is shown to be small in all but the smallest basis sets for recommended grid sizes. This study also reports the assessment of VV10-containing functionals for predicting harmonic frequencies using the analytical second derivative code. The contribution of VV10 to simulating harmonic frequencies is shown to be small for small molecules but important for systems where weak interactions are important, such as water clusters. In the latter cases, B97M-V, ωB97M-V, and ωB97X-V perform very well. The convergence of frequencies with respect to grid size and atomic orbital basis set size is studied and recommendations reported. Finally, scaling factors to allow comparison of scaled harmonic frequencies with experimental fundamental frequencies and to predict zero-point vibrational energy are presented for some recently developed functionals (including r2SCAN, B97M-V, ωB97X-V, M06-SX, and ωB97M-V).

I. INTRODUCTION

Density functional theory (DFT) is currently the most popular approach to predicting molecular properties, such as relative energies, equilibrium geometries, frequencies, excitation energies, permanent and induced moments, etc.[1–4] However, standard semi-local exchange-correlation functionals cannot properly account for the long-range correlation effects such as dispersion (van der Waals) interactions.[5–8] A range of methods have been developed to address this issue.[9,10] One popular, effective, and computationally very inexpensive strategy to fix the problem is adding an empirical dispersion correction, such as the exchange-dipole model (XDM)[11], the Tkatchenko-Scheffler van der Waals method[12] and the DFT-D family.[13–16] However, strictly speaking, these methods are not density functionals, as they depend explicitly on nuclear positions. The most elaborate methods are orbital-dependent, like the random-phase approximation (RPA)[17–19] and double-hybrid density functionals,[20,21] but they are very time-demanding. To strike an intermediate balance between rigor and computational tractability, researchers have devised a series of nonlocal correlation functionals that aim to capture only long-range dispersion effects. The first was the well-known vdW-DF functional,[22] which was designed in 2004, followed by vdW-DF2 in 2010.[23] Vydrov and Van Voorhis also proposed the VV09 functional[24] and its more successful successor, VV10,[25] for the calculation of dispersion-containing interactions in molecules.

VV10 has since been widely used as an add-on to existing functionals.[10,16,25,26] Furthermore, VV10 has been incorporated as a component in self-consistently training new functionals, such as ωB97X-V[27] [range-separated hybrid (RSH) generalized-gradient approximation (GGA)], B97M-V[28] [local meta-GGA (mGGA)], and ωB97M-V[29] (RSH mGGA). Their success has been demonstrated by improved accuracy in predicting energy differences across broad classes of molecules composed of main group elements, with particular improvements noted for intermolecular interactions[1,8,29] In addition, for applications in condensed matter, VV10 was reformulated, leading to the closely related rVV10 functional,[30] which offers significant implementation advantages in periodic codes, while yielding virtually identical results.

Analytical derivative theory[31,32] has long been essential for exploring potential energy surfaces using electronic structure methods. Indeed, the analytical gradient of VV10 is widely available, enabling geometry optimizations. Building on the theory of Hartree-Fock second derivatives[33,34], efficient algorithms and implementations of DFT analytical second derivatives are well established,[35–37] with some development continuing.[38–40] However, to the best of our

knowledge, the VV10 analytical second derivative has not yet been implemented in any quantum chemistry software. There has been recent interest in analytic derivatives through automatic differentiation[41,42] or symbolic algebra,[43–46] but VV10 Hessians have not been reported that way either, possibly due to its complexity (as shown in this paper and similarly for vdW-DF[47,48]). In this context, the finite difference (FD) method has to be employed for frequency,[49] excitation energy, and stability analysis calculations.[50] Even though the FD approach approximates analytical methods, it has more limited precision and may require significantly more computational resources. Therefore, analytical derivatives are typically preferred when feasible, and the first purpose of this paper is to report the theory and implementation of VV10 analytical second derivatives.

Nowadays many functionals have been benchmarked extensively for predicting frequencies and zero-point vibrational energies (ZPVEs).[51–65] Most of these works calculated harmonic frequencies with a scaling factor to fit experimental frequencies or ZPVEs, which accords with practical usage, but introduces an additional error in benchmarking.[51–63] In this scenario, B3LYP is good enough to consistently provides the best (or near-best) results among hybrid functionals.[56–58] For detailed reviews on the topic, please consult refs. 2, 3, and 63. By contrast, relatively few papers have compared harmonic frequencies with theoretical best estimates (TBEs), so as to directly assess the accuracy of functionals themselves.[54,65] Here, as our second purpose, we will benchmark B97M-V, ωB97X-V, and ωB97M-V with other popular functionals mainly against TBEs to avoid errors from other sources. Finally, at the end will we employ experimental reference values to develop scaling factors for recently developed functionals (including r2SCAN, B97M-V, ωB97X-V, M06-SX, and ωB97M-V).

In this paper, we will describe the theory and implementation of the second analytical derivatives of VV10-containing functionals (Section II), including orbital Hessian, nuclear Hessian, and Fock nuclear derivative contributions. We have already discussed the contribution of VV10 to excitation energies,[4] so we only benchmark the performance of B97M-V, ωB97X-V, and ωB97M-V for simulating molecular frequencies here. We will benchmark the computational time (Section III B), explore the basis set and quadrature grid convergence (Section IV A), study the contribution of VV10 to frequency prediction (Section IV B), compare VV10-containing functionals with other popular functionals against TBEs on various data sets (Section IV C), and finally recommend scaling factors to employ in practice (Section IV D).

II. THEORY AND IMPLEMENTATION OF VV10

A. VV10 Energy and First Derivative

The energy of the nonlocal correlation functional, VV10, can be written as (here we use atomic units)

$$E^{\mathrm{VV10}} = \int d^3\mathbf{r}\,\rho(\mathbf{r})\Big[\beta + \frac{1}{2}\int d^3\mathbf{r}'\,\rho(\mathbf{r}')\Phi(\mathbf{r},\mathbf{r}')\Big], \tag{1}$$

where $\rho(\mathbf{r})$ is the total electron density and $\Phi(\mathbf{r},\mathbf{r}')$ is the correlation kernel defined as

$$\Phi = -\frac{3}{2gg'(g+g')} \tag{2}$$

with

$$\begin{aligned} g(\mathbf{r},\mathbf{r}') &= \omega(\mathbf{r})|\mathbf{r}-\mathbf{r}'|^2 + \kappa(\mathbf{r}), \\ g'(\mathbf{r},\mathbf{r}') &= \omega(\mathbf{r}')|\mathbf{r}-\mathbf{r}'|^2 + \kappa(\mathbf{r}'). \end{aligned} \tag{3}$$

$\omega(\mathbf{r})$ and $\kappa(\mathbf{r})$ are both intermediate single-variable functions, defined as

$$\omega(\mathbf{r}) = \sqrt{C\frac{\gamma(\mathbf{r})^2}{\rho(\mathbf{r})^4} + \frac{4\pi\rho(\mathbf{r})}{3}}, \tag{4}$$

$$\kappa(\mathbf{r}) = b\frac{3\pi}{2}\left(\frac{\rho(\mathbf{r})}{9\pi}\right)^{\frac{1}{6}}, \tag{5}$$

where $\gamma = |\nabla\rho|^2$ is the square of the density gradient and b and C are two parameters that control the behavior of VV10. For the detailed physical meaning of each variable, please consult the original paper.[25] The correction β in Eq 1 is also determined by b to ensure that the VV10 energy is equal to 0 in the uniform density limit,

$$\beta = \frac{1}{32}\left(\frac{3}{b^2}\right)^{\frac{3}{4}}. \tag{6}$$

To evaluate the VV10 functional on a quadrature grid (for example the widely used atom-centered method pioneered by Becke[66]), we adopt the following formalism. The energy can be calculated as

$$E^{\mathrm{VV10}} = \sum_i w_i f_i^0, \tag{7}$$

$$f_i^0 = \rho_i\big(\beta + \frac{1}{2}\mathrm{E}_i\big), \tag{8}$$

$$\mathrm{E}_i = \sum_j w_j \rho_j \Phi_{ij}, \tag{9}$$

$$\Phi_{ij} = -\frac{3}{2 g_{ij} g'_{ij} (g_{ij} + g'_{ij})}. \tag{10}$$

Here the subscript i indicates that the value is at the i-th (outer) grid point. For example, w_i is the quadrature weight of the i-th grid point and f_i^0 is the VV10 (outer) integrand at this quadrature point. E_i is an intermediate variable representing the inner integral of Eq 1 at point i. Similarly, j indicates that the value is at the j-th (inner) grid point. $g_{ij} = \omega_i {R^2}_{ij} + \kappa_i$, $g'_{ij} = \omega_j {R^2}_{ij} + \kappa_j$, and ${R^2}_{ij} = |\mathbf{r}_i - \mathbf{r}_j|^2$ are corresponding to Eq 2 and 3. It is worth noting $g'_{ij} = g_{ji}$ but we keep the index j as the fast index throughout the implementation.

The VV10 contribution to the Fock matrix can be calculated by

$$F_{\mu\nu} = \sum_i w_i \Big[f_i^\rho \phi_{\mu i} \phi_{\nu i} + 2 f_i^\gamma \nabla \rho_i \cdot (\phi_{\nu i} \nabla \phi_{\mu i} + \phi_{\mu i} \nabla \phi_{\nu i}) \Big], \tag{11}$$

$$f_i^\rho = \beta + \mathrm{E}_i + \rho_i \Big[(\frac{\partial \kappa}{\partial \rho})_i \mathrm{U}_i + (\frac{\partial \omega}{\partial \rho})_i \mathrm{W}_i \Big], \tag{12}$$

$$f_i^\gamma = \rho_i (\frac{\partial \omega}{\partial \gamma})_i \mathrm{W}_i. \tag{13}$$

$\phi_{\mu i}$ and $\phi_{\nu i}$ are the values of atomic orbitals ϕ_μ and ϕ_ν at the quadrature point i. We use real functions and thus omit complex conjugations for simplicity. ∇ without any subscript stands for the gradient with respect to the electron position. f_i^ρ and f_i^γ are the partial derivatives of the outer integrand at point i with respect to ρ_i and γ_i individually. $(\frac{\partial \kappa}{\partial \rho})_i$, $(\frac{\partial \omega}{\partial \rho})_i$, and $(\frac{\partial \omega}{\partial \gamma})_i$ are also the partial derivatives of κ and ω. U_i and W_i are two intermediate integral values similar to E_i, which are defined as

$$\mathrm{U}_i = -\sum_j w_j \rho_j \Phi_{ij} (\frac{1}{g_{ij} + g'_{ij}} + \frac{1}{g_{ij}}), \tag{14}$$

$$\mathrm{W}_i = -\sum_j w_j \rho_j \Phi_{ij} {R^2}_{ij} (\frac{1}{g_{ij} + g'_{ij}} + \frac{1}{g_{ij}}). \tag{15}$$

We split the VV10 gradient into three terms:

$$E^A = \nabla_A E = E_G^A + E_w^A + E_{gr}^A. \tag{16}$$

Here A stands for one cartesian coordinate (i.e., x, y, or z) of one atom. E_G^A, E_w^A, E_{gr}^A denote the contributions from the change of Gaussian basis functions, quadrature weights, and grid positions respectively.

$$E_G^A = \sum_i w_i [f_i^\rho \rho_i^A + f_i^\gamma \gamma_i^A], \tag{17}$$

$$E_w^A = \sum_i w_i^A \rho_i \big(\beta + \mathrm{E}_i\big), \tag{18}$$

$$\begin{aligned}
E_{gr}^A =& -\sum_{i\in A}\sum_{j\notin A} w_i w_j \rho_i \rho_j \Phi_{ij} \left(\frac{\omega_i}{g_{ij}} + \frac{\omega_j}{g'_{ij}} + \frac{\omega_i+\omega_j}{g_{ij}+g'_{ij}}\right)(\mathbf{r}_i - \mathbf{r}_j) \\
& -\sum_{i\notin A}\sum_{j\in A} w_i w_j \rho_i \rho_j \Phi_{ij} \left(\frac{\omega_i}{g_{ij}} + \frac{\omega_j}{g'_{ij}} + \frac{\omega_i+\omega_j}{g_{ij}+g'_{ij}}\right)(\mathbf{r}_j - \mathbf{r}_i) \\
=& -2\sum_{i\in A}\sum_{j\notin A} w_i w_j \rho_i \rho_j \Phi_{ij} \left(\frac{\omega_i}{g_{ij}} + \frac{\omega_i}{g_{ij}+g'_{ij}}\right)(\mathbf{r}_i - \mathbf{r}_j) \\
& -2\sum_{i\notin A}\sum_{j\in A} w_i w_j \rho_i \rho_j \Phi_{ij} \left(\frac{\omega_j}{g'_{ij}} + \frac{\omega_j}{g_{ij}+g'_{ij}}\right)(\mathbf{r}_j - \mathbf{r}_i).
\end{aligned} \tag{19}$$

Here w_i^A, ρ_i^A, and γ_i^A are the gradient of w_i, ρ_i, and γ_i with respect to the change of A. The calculation time of Eq 19 can be saved half by translational invariance. Eq 19 can also be written in the form of Eq 44,

$$E_{gr}^A = \sum_{i\in A} w_i \rho_i E_i^{Agr} \tag{20}$$

B. Second Derivative

To simulate the molecular frequencies by coupled self-consistent field theory (CPSCF), we need several key quantities. The first quantity contains the orbital Hessian contributions (the second derivative of the VV10 energy with respect to the density matrix, which is also needed for time-dependent density functional theory (TDDFT) to predict the excitation energy.[4]). Usually, we only calculate contracted orbital Hessian $G^t_{\mu\nu}$, to avoid the fourth-rank tensor storage of orbital Hessian. The second quantity is the nuclear Hessian, E^{AB}, which is the second derivative of the VV10 energy with respect to nuclear positions. The third quantity is the Fock nuclear derivative $F^A_{\mu\nu}$, which is the derivative of the VV10 contribution to the Fock matrix with respect to nuclear position.

The contracted orbital Hessian term $G^t_{\mu\nu}$ defined in Eq 9 of ref 4 can be calculated by

$$G^t_{\mu\nu} = \sum_i w_i \Big[f_i^{\rho,t} \phi_{\mu i}\phi_{\nu i} + 2[f_i^{\gamma,t}\nabla\rho_i + f_i^{\gamma}\nabla\rho_i^t]\cdot(\phi_{\nu i}\nabla\phi_{\mu .i} + \phi_{\mu i}\nabla\phi_{\nu i})\Big], \tag{21}$$

$$\begin{aligned}
f_i^{\rho,t} =& \sum_j w_j (f_{ij}^{\rho\rho}\rho_j^t + 2 f_{ij}^{\rho\gamma}\gamma_j^t), \\
f_i^{\gamma,t} =& \sum_j w_j (f_{ij}^{\gamma\rho}\rho_j^t + 2 f_{ij}^{\gamma\gamma}\gamma_j^t).
\end{aligned} \tag{22}$$

ρ_i^t and γ_i^t are the trial electron density and trial gamma density on i-th grid point, which are defined as

$$\rho_i^t = \Sigma_{\mu\nu} P_{\mu\nu}^t \phi_{\mu i} \phi_{\nu i}, \quad \gamma_i^t = \nabla\rho_i \cdot \nabla\rho_i^t, \quad \nabla\rho_i^t = \Sigma_{\mu\nu} P_{\mu\nu}^t \nabla(\phi_{\mu i}\phi_{\nu i}). \tag{23}$$

$P_{\mu\nu}^t$ is the trial density matrix defined in Eq 8 of ref 4.

$f^{\rho\rho}$, $f^{\rho\gamma}$, $f^{\gamma\rho}$ and $f^{\gamma\gamma}$ in Eq 22 are all the second derivatives of the VV10 energy, which can be calculated by

$$\begin{aligned} f_{ij}^{\rho\rho} = \frac{\partial^2 E^{\mathrm{VV10}}}{\partial\rho_i \partial\rho_j} &= \Phi_{ij}\Big\{\rho_i\Big(R^2{}_{ij}(\frac{\partial\omega}{\partial\rho})_i + (\frac{\partial\kappa}{\partial\rho})_i\Big)\rho_j\Big(R^2{}_{ij}(\frac{\partial\omega}{\partial\rho})_j + (\frac{\partial\kappa}{\partial\rho})_j\Big)\Big(\frac{2}{(g_{ij}+g'_{ij})^2} + \frac{2}{g_{ij}g'_{ij}}\Big) \\ &- \rho_i\Big(R^2{}_{ij}(\frac{\partial\omega}{\partial\rho})_i + (\frac{\partial\kappa}{\partial\rho})_i\Big)(\frac{1}{g_{ij}+g'_{ij}} + \frac{1}{g_{ij}}) - \rho_j\Big(R^2{}_{ij}(\frac{\partial\omega}{\partial\rho})_j + (\frac{\partial\kappa}{\partial\rho})_j\Big)(\frac{1}{g_{ij}+g'_{ij}} + \frac{1}{g'_{ij}}) + 1\Big\} \\ &+ \frac{\delta_{ij}}{w_i}\Big\{\ \Big[2(\frac{\partial\omega}{\partial\rho})_i \mathrm{W}_i + 2(\frac{\partial\kappa}{\partial\rho})_i \mathrm{U}_i\Big] + \rho_i\Big[(\frac{\partial^2\omega}{\partial\rho^2})_i \mathrm{W}_i + (\frac{\partial^2\kappa}{\partial\rho^2})_i \mathrm{U}_i \\ &+ (\frac{\partial\kappa}{\partial\rho})_i(\frac{\partial\kappa}{\partial\rho})_i \mathrm{A}_i + (\frac{\partial\omega}{\partial\rho})_i(\frac{\partial\omega}{\partial\rho})_i \mathrm{C}_i + 2(\frac{\partial\omega}{\partial\rho})_i(\frac{\partial\kappa}{\partial\rho})_i \mathrm{B}_i\Big]\ \Big\}, \end{aligned} \tag{24}$$

$$\begin{aligned} f_{ij}^{\gamma\rho} = \frac{\partial^2 E^{\mathrm{VV10}}}{\partial\gamma_i \partial\rho_j} &= \rho_i(\frac{\partial\omega}{\partial\gamma})_i R^2{}_{ij}\Phi_{ij}\Big[\rho_j\Big(R^2{}_{ij}(\frac{\partial\omega}{\partial\rho})_j + (\frac{\partial\kappa}{\partial\rho})_j\Big)\Big(\frac{2}{(g_{ij}+g'_{ij})^2} + \frac{2}{g_{ij}g'_{ij}}\Big) - (\frac{1}{g_{ij}+g'_{ij}} + \frac{1}{g_{ij}})\Big] \\ &+ \frac{\delta_{ij}}{w_i}\Big[(\frac{\partial\omega}{\partial\gamma})_i \mathrm{W}_i + \rho_i(\frac{\partial^2\omega}{\partial\gamma\partial\rho})_i \mathrm{W}_i + \rho_i(\frac{\partial\omega}{\partial\gamma})_i(\frac{\partial\kappa}{\partial\rho})_i \mathrm{B}_i + \rho_i(\frac{\partial\omega}{\partial\gamma})_i(\frac{\partial\omega}{\partial\rho})_i \mathrm{C}_i\Big], \end{aligned} \tag{25}$$

$$\begin{aligned} f_{ij}^{\rho\gamma} = \frac{\partial^2 E^{\mathrm{VV10}}}{\partial\rho_i \partial\gamma_j} &= \rho_j(\frac{\partial\omega}{\partial\gamma})_j R^2{}_{ij}\Phi_{ij}\Big[\rho_i\Big(R^2{}_{ij}(\frac{\partial\omega}{\partial\rho})_i + (\frac{\partial\kappa}{\partial\rho})_i\Big)\Big(\frac{2}{(g'_{ij}+g_{ij})^2} + \frac{2}{g'_{ij}g_{ij}}\Big) - (\frac{1}{g'_{ij}+g_{ij}} + \frac{1}{g'_{ij}})\Big] \\ &+ \frac{\delta_{ij}}{w_i}\Big[(\frac{\partial\omega}{\partial\gamma})_i \mathrm{W}_i + \rho_i(\frac{\partial^2\omega}{\partial\gamma\partial\rho})_i \mathrm{W}_i + \rho_i(\frac{\partial\omega}{\partial\gamma})_i(\frac{\partial\kappa}{\partial\rho})_i \mathrm{B}_i + \rho_i(\frac{\partial\omega}{\partial\gamma})_i(\frac{\partial\omega}{\partial\rho})_i \mathrm{C}_i\Big], \end{aligned} \tag{26}$$

$$\begin{aligned} f_{ij}^{\gamma\gamma} = \frac{\partial^2 E^{\mathrm{VV10}}}{\partial\gamma_i \partial\gamma_j} &= \rho_i\rho_j(\frac{\partial\omega}{\partial\gamma})_i(\frac{\partial\omega}{\partial\gamma})_j(R^2{}_{ij})^2\Phi_{ij}(\frac{2}{(g_{ij}+g'_{ij})^2} + \frac{2}{g_{ij}g'_{ij}}) \\ &+ \frac{\delta_{ij}}{w_i}\rho_i((\frac{\partial^2\omega}{\partial\gamma^2})_i \mathrm{W}_i + (\frac{\partial\omega}{\partial\gamma})^2 \mathrm{C}_i). \end{aligned} \tag{27}$$

Here, A_i, B_i and C_i are integrals that are similar to U_i and W_i:

$$\mathrm{A}_i = \sum_j 2w_j\rho_j\Phi_{ij}(\frac{1}{(g_{ij}+g'_{ij})^2} + \frac{1}{(g_{ij}+g'_{ij})g_{ij}} + \frac{1}{g_{ij}^2}), \tag{28}$$

$$\mathrm{B}_i = \sum_j 2w_j\rho_j\Phi_{ij}R^2{}_{ij}(\frac{1}{(g_{ij}+g'_{ij})^2} + \frac{1}{(g_{ij}+g'_{ij})g_{ij}} + \frac{1}{g_{ij}^2}), \tag{29}$$

$$\mathrm{C}_i = \sum_j 2w_j\rho_j\Phi_{ij}(R^2{}_{ij})^2\left(\frac{1}{(g_{ij}+g'_{ij})^2}+\frac{1}{(g_{ij}+g'_{ij})g_{ij}}+\frac{1}{g_{ij}^2}\right). \tag{30}$$

Similarly to the nuclear gradient, the nuclear Hessian can be split into nine terms:

$$\begin{aligned} E^{AB} =& \nabla_B\nabla_A E \\ =& E^{AB}_{G,G}+E^{AB}_{w,w}+E^{AB}_{gr,gr}+E^{AB}_{w,G}+E^{AB}_{gr,G}+E^{AB}_{G,w}+E^{AB}_{gr,w}+E^{AB}_{G,gr}+E^{AB}_{w,gr} \\ =& E^{AB}_{G,G}+E^{AB}_{w,w}+E^{AB}_{gr,gr}+E^{AB}_{w,G}+(E^{AB}_{w,G})^\intercal+E^{AB}_{gr,G}+(E^{AB}_{gr,G})^\intercal+E^{AB}_{gr,w}+(E^{AB}_{gr,w})^\intercal. \end{aligned} \tag{31}$$

$$E^{AB}_{w,w} = \sum_i (w_i^{AB})\rho_i\left(\beta+\mathrm{E}_i\right)+\sum_i w_i^A\otimes\rho_i\mathrm{E}_i^{Bw}, \tag{32}$$

$$E^{AB}_{w,gr} = \sum_i w_i^A\otimes\rho_i\mathrm{E}_i^{Bgr}, \tag{33}$$

$$E^{AB}_{G,w} = \sum_i w_i^B\otimes[f_i^\rho\rho_i^A+f_i^\gamma\gamma_i^A] \tag{34}$$

$$+\sum_i w_i\rho_i^A\otimes\left[\mathrm{E}_i^{Bw}+\rho_i[(\frac{\partial\kappa}{\partial\rho})_i\mathrm{U}_i^{Bw}+(\frac{\partial\omega}{\partial\rho})_i\otimes\mathrm{W}_i^{Bw}]\right] \tag{35}$$

$$+\sum_i w_i\gamma_i^A\otimes\rho_i(\frac{\partial\omega}{\partial\gamma})_i\mathrm{W}_i^{Bw}, \tag{36}$$

$$E^{AB}_{G,gr} = \sum_i w_i\rho_i^A\otimes\left[\mathrm{E}_i^{Bgr}+\rho_i[(\frac{\partial\kappa}{\partial\rho})_i\mathrm{U}_i^{Bgr}+(\frac{\partial\omega}{\partial\rho})_i\mathrm{W}_i^{Bgr}]\right] \tag{37}$$

$$+\sum_i w_i\gamma_i^A\otimes\rho_i(\frac{\partial\omega}{\partial\gamma})_i\mathrm{W}_i^{Bgr}, \tag{38}$$

$$E^{AB}_{gr,gr} = \sum_{i\in A} w_i\rho_i\mathrm{D}_i^B \text{ if } A\neq B \text{ and } E^{AA}_{gr,gr} = -\sum_{B\neq A} E^{AB}_{gr,gr}, \tag{39}$$

$$E^{AB}_{G,G} = \sum_i w_i\left[f_i^\rho\rho_i^{AB}+f_i^\gamma\gamma_i^{AB}+\rho_i^A\otimes\sum_j w_j(f_{ij}^{\rho\rho}\rho_j^B+f_{ij}^{\rho\gamma}\gamma_j^B)+\gamma_i^A\otimes\sum_j w_j(f_{ij}^{\gamma\rho}\rho_j^B+f_{ij}^{\gamma\gamma}\gamma_j^B)\right]. \tag{40}$$

w_i^{AB}, ρ_i^{AB}, and γ_i^{AB} are the Hessian of w_i, ρ_i, and γ_i with respect to the change of atoms A and B. E_i^{Bw}, E_i^{Uw}, E_i^{Ww}, E_i^{Bgr}, E_i^{Ugr}, and E_i^{Wgr} are all integrals in the form of three-element vectors (for x, y, z directions). D_i is a three-by-three matrix. They can be calculated through the following equations.

$$\mathrm{E}_i^{Bw} = \sum_j w_j^B \rho_j \Phi_{ij}, \tag{41}$$

$$\mathrm{U}_i^{Bw} = -\sum_j w_j^B \rho_j \Phi_{ij} \left(\frac{1}{g_{ij}+g'_{ij}} + \frac{1}{g_{ij}}\right), \tag{42}$$

$$\mathrm{W}_i^{Bw} = -\sum_j w_j^B \rho_j \Phi_{ij} R^2{}_{ij} \left(\frac{1}{g_{ij}+g'_{ij}} + \frac{1}{g_{ij}}\right), \tag{43}$$

$$\mathrm{E}_i^{Bgr} = \begin{cases} -2\sum_{j\in B} w_j \rho_j \Phi_{ij} \left(\frac{\omega_i}{g_{ij}} + \frac{\omega_j}{g'_{ij}} + \frac{\omega_i+\omega_j}{g_{ij}+g'_{ij}}\right)(\mathbf{r}_j - \mathbf{r}_i), & i \notin B \\ -\sum_{C\neq B} \mathrm{E}_i^{Cgr}, & i \in B \end{cases} \tag{44}$$

$$\mathrm{U}_i^{Bgr} = \begin{cases} 2\sum_{j\in B} w_j \rho_j \Phi_{ij} \Big[\left(\frac{\omega_i}{g_{ij}} + \frac{\omega_j}{g'_{ij}} + \frac{\omega_i+\omega_j}{g_{ij}+g'_{ij}}\right)\left(\frac{1}{g_{ij}+g'_{ij}} + \frac{1}{g_{ij}}\right) \\ + \left(\frac{\omega_i}{g_{ij}^2} + \frac{\omega_i+\omega_j}{(g_{ij}+g'_{ij})^2}\right)\Big](\mathbf{r}_j - \mathbf{r}_i), & i \notin B \\ -\sum_{C\neq B} \mathrm{U}_i^{Cgr}, & i \in B \end{cases} \tag{45}$$

$$\mathrm{W}_i^{Bgr} = \begin{cases} 2\sum_{j\in B} w_j \rho_j \Phi_{ij} \Big[R^2{}_{ij} \left(\frac{\omega_i}{g_{ij}} + \frac{\omega_j}{g'_{ij}} + \frac{\omega_i+\omega_j}{g_{ij}+g'_{ij}}\right)\left(\frac{1}{g_{ij}+g'_{ij}} + \frac{1}{g_{ij}}\right) \\ + R^2{}_{ij}\left(\frac{\omega_i}{g_{ij}^2} + \frac{\omega_i+\omega_j}{(g_{ij}+g'_{ij})^2}\right) - \left(\frac{1}{g_{ij}+g'_{ij}} + \frac{1}{g_{ij}}\right)\Big](\mathbf{r}_j - \mathbf{r}_i), & i \notin B \\ -\sum_{C\neq B} \mathrm{W}_i^{Cgr}, & i \in B \end{cases} \tag{46}$$

$$\begin{aligned} \mathrm{D}_i^B = -2\sum_{j\in B} w_j \rho_j \Phi_{ij} \Bigg[2\Big[&\left(\frac{\omega_i}{g_{ij}} + \frac{\omega_j}{g'_{ij}} + \frac{\omega_i+\omega_j}{g_{ij}+g'_{ij}}\right)^2 + \left(\frac{\omega_i}{g_{ij}}\right)^2 + \left(\frac{\omega_j}{g'_{ij}}\right)^2 \\ &+ \left(\frac{\omega_i+\omega_j}{g_{ij}+g'_{ij}}\right)^2\Big](\mathbf{r}_j - \mathbf{r}_i) \otimes (\mathbf{r}_j - \mathbf{r}_i) - \left(\frac{\omega_i}{g_{ij}} + \frac{\omega_j}{g'_{ij}} + \frac{\omega_i+\omega_j}{g_{ij}+g'_{ij}}\right)\mathbf{I}_3 \Bigg], \quad i \notin B \end{aligned} \tag{47}$$

Here the symbol $\otimes$ represents the outer product of two vectors and $\mathbf{I}_3$ is the three-by-three identity matrix.

The nuclear derivative of the Fock matrix can be also split into three terms:

$$F^A_{\mu\nu} = \nabla_A F_{\mu\nu} = F^A_{\mu\nu,G} + F^A_{\mu\nu,w} + F^A_{\mu\nu,gr}, \tag{48}$$

$$\begin{aligned} F^A_{\mu\nu,G} = &\sum_i w_i \Big[f_i^\rho \nabla_A (\phi_\mu \phi_\nu)_i + 2 f_i^\gamma \nabla_A [\nabla\rho \cdot \nabla(\phi_\mu \phi_\nu)]_i \Big] \\ &+ \sum_i w_i \Big[\phi_{\mu i}\phi_{\nu i} \sum_j w_j [f_{ij}^{\rho\rho} \rho_j^A + f_{ij}^{\rho\gamma} \gamma_j^A] + 2(\nabla\rho)_i \cdot [\nabla(\phi_\mu\phi_\nu)]_i \sum_j w_j [f_{ij}^{\gamma\rho} \rho_j^A + f_{ij}^{\gamma\gamma} \gamma_j^A] \Big], \end{aligned} \tag{49}$$

$$\begin{aligned} F^A_{\mu\nu,gr} = &\sum_i w_i \phi_{\mu i}\phi_{\nu i} \Big[\mathbf{E}_i^{Bgr} + \rho_i [(\frac{\partial \boldsymbol{\kappa}}{\partial \rho})_i \mathbf{U}_i^{Bgr} + (\frac{\partial \omega}{\partial \rho})_i \mathbf{W}_i^{Bgr}] \Big] \\ &+ 2\sum_i w_i (\nabla\rho)_i \cdot [\nabla(\phi_\mu\phi_\nu)]_i \rho_i (\frac{\partial \omega}{\partial \gamma})_i \mathbf{W}_i^{Bgr}, \end{aligned} \tag{50}$$

$$
\begin{aligned}
F^A_{\mu\nu,w} = &\sum_i (\nabla_A w_i)\Big[f_i^{\rho}\phi_{\mu i}\phi_{\nu i} + 2f_i^{\gamma}(\nabla\rho)_i \cdot [\nabla(\phi_\mu\phi_\nu)]_i\Big] \\
&+ \sum_i w_i\phi_{\mu i}\phi_{\nu i}\left[\mathbf{E}_i^{Aw} + \rho_i\Big[(\frac{\partial\kappa}{\partial\rho})_i\mathbf{U}_i^{Aw} + (\frac{\partial\omega}{\partial\rho})_i\mathbf{W}_i^{Aw}\Big]\right] \\
&+ 2\sum_i w_i(\nabla\rho)_i \cdot [\nabla(\phi_\mu\phi_\nu)]_i\Big[\rho_i(\frac{\partial\omega}{\partial\gamma})_i\mathbf{W}_i^{Aw}\Big],
\end{aligned}
\tag{51}
$$

where the dot symbol $\cdot$ represents the dot product of two vectors.

When implementing the equations above, we have adopted some important optimizations to improve efficiency. For example, translational invariance is employed to avoid or minimize some computationally heavy tasks, like the computations of $w_i^A\,(i \in A)$, $\mathrm{E}_i^{Bgr}\,(i \in B)$, and $E^{AA}_{gr,gr}$. Grid screening technology is also used to avoid unnecessary calculations like $\sum_j w_j[f_{ij}^{\rho\rho}\rho_j^B + f_{ij}^{\rho\gamma}\gamma_j^B]$ when ρ^B and γ^B are under the precision threshold in this batch of j.

III. COMPUTATIONAL DETAILS AND TIME BENCHMARK

A. Computational details

We have selected a range of widely used density functionals, as well as a set of density functionals containing the VV10 functional for the assessment of predicted frequencies. The tested density functionals include

1. GGA (Rung 2): B97-D[13], PBE[67];
2. mGGA (Rung 3): B97M-V[28], SCAN[68], r2SCAN[69], M06-L[70];
3. hybrid GGA (Rung 4a): ωB97X-D[71], CAM-B3LYP[72], ωB97X-V[27], HSE-HJS[73,74], B3LYP[75,76];
4. hybrid mGGA (Rung 4b): BMK[77], M06-SX[78], M06-2X[79], ωB97M-V[29], SCAN0[80].

The D3(BJ) empirical correction[15] is added to any functional without its own dispersion component.

We benchmarked the performance of these functionals for predicting harmonic frequency TBEs on the data sets shown in Table I and used their theoretical best geometries (TBGs) as the starting geometries of the optimization.

Q-Chem 5.4 and Q-Chem 6.0 were used to perform all of the calculations.[93] In Section IV A, the def2 basis set family[94,95] (def2-SVP, def2-SVPD, def2-TZVP, def2-TZVPD, def2-QZVPP, and

TABLE I: Summary of data sets used for benchmarking the performance of density functionals for predicting harmonic frequencies.

Data set	Subset Name	Computational method to generate TBEs	Computational method to generate TBGs	Number of molecules (or conformations)	Number of frequencies
Covalent Set	HFREQ2014[81,a]	CCSD(T*)-F12c/cc-pVQZ-F12	CCSD(T*)-F12c/cc-pVQZ-F12	30	112
	Diatomic[82,b]	CCSD(T)(:κ-OOMP2)[c]/ aug-cc-pwCVTZ[84,85]	CCSD(T)(:κ-OOMP2)/ aug-cc-pwCVTZ	70	70
Noncovalent Set	H2O[86,d]	CCSD(T):MP2[e]/haQZ[f]	CCSD(T):MP2/haQZ	7	282
	V30[88,g]	CCSD(T)/haQZ	CCSD(T)/haQZ	30	331
	H2S[89,h]	CCSD(T)/aug-cc-pVQZ	CCSD(T)/aug-cc-pVQZ	1	12
	N2O[90,i]	CCSD(T)-F12b/cc-pVQZ-F12[j]	CCSD(T)-F12b/cc-pVQZ-F12	4	36
	CO2[91,k]	CCSD(T)-F12b/cc-pVTZ-F12	CCSD(T)-F12b/cc-pVTZ-F12	2	24
	P[92,l]	CCSD(T)/aug-cc-pVTZ	CCSD(T)/aug-cc-pVTZ	5	79
		At total		149	946

[a] A set of common small molecules with high-quality benchmark values. We discarded the CH_3OH molecule because its geometry is not reported clearly in the original paper.

[b] A set of diatomic molecules containing more diverse elements than the HFREQ2014 set. We split it into a restricted subset (DiatomicR, which has 25 frequencies) and an unrestricted subset (DiatomicU, which has 45 frequencies).

[c] CCSD(T) based on κ-OOMP2 orbitals.[83]

[d] A set of water clusters ranging in size from the trimer to four different isomers of the hexamer.

[e] 2-body:Many-body CCSD(T):MP2 theory[87]

[f] aug-cc-pVQZ basis set for non-hydrogen atoms and cc-pVQZ for hydrogen atoms.

[g] A set of molecular dimers with different polarity combinations (polar-polar, polar-nonpolar, and nonpolar-nonpolar).

[h] H_2S dimer.

[i] A set of 4 dimers incorporating N_2O.

[j] O_2-N_2O is an exception which is calculated by UCCSD(T)-F12b/cc-pVTZ-F12 method.

[k] CO_2-CO dimer and CO_2-NH_3 dimer that are not in the V30 set

[l] A set of P_2 dimer and PCCP dimers in different point group symmetries.

def2-QZVPPD) is used to study the basis set convergence, and the standard grids[96,97] (SG-0/1/2/3) in Q-Chem and their parents [(23, 170), (50, 194), (75, 302), (99, 590)] are used to study the grid convergence. Here (X, Y) means a radial grid with X points and an angular Lebedev grid with Y points. After that, all the calculations employ the (99,590) grid for local functional (XC) integrals and SG-1 for nonlocal VV10 correlation (NL).

It is worth noting that optimizing the geometries of molecules in the Noncovalent Set proved to be quite challenging due to obtaining imaginary frequencies at a fraction of the optimized geometries. To eliminate imaginary frequencies, we have attempted a variety of techniques to refine the optimized geometries, including altering convergence thresholds, employing the exact Hessian, perturbing the geometries, and so on. The details are described in the Supporting Information.

B. Time benchmark

As described in Section II B, we can divide a frequency job into different computational tasks: self-consistent field (SCF) energy, orbital Hessian contributions (G), nuclear Hessian (Hess), and Fock nuclear derivative (F_{nuc}). For each task, we need to construct matrix contributions from the XC, NL, and Coulomb and HF exchange (JK) parts individually. Here we report the parallel efficiency and time scaling with respect to basis set size and molecule size for ωB97M-V frequency calculations in our implementation. All timing jobs were run on a single Haswell node of the NERSC supercomputer. Each Haswell node (Intel Xeon Processor E5-2698 v3) has two sockets, each populated with a 2.3 GHz 16-core Haswell processor. These timings reflect OpenMP performance up to 32 physical cores, as well as system-size scaling for our current implementation.

From Figure 1(a), the parallel efficiency of the NL part is as good as for the XC part and we can still get an appreciable speedup between 16 and 32 physical cores. While it is not the topic of this work, we see that the parallel efficiency of the JK terms is not good, and suggests that these codes would benefit from restructuring. Figure 1(b) and 1(c) displays the elapsed time of those tasks which take more than 1% of total wall time. It is clear that only the orbital Hessian (G) of the NL part takes more than 1% of the total wall time. Encouragingly, this is still less than the XC part and likewise is less than 10% of total wall time except for the smallest basis set, 6-31G*. The total wall time and time scaling are both dominated by the JK part, which appears to reflect its relatively poor parallel scaling as already discussed.

From Figure 1(b) and Table S1.1, we can see that the elapsed time for the NL part of all tasks grows sublinearly with respect to the number of basis functions (N_{basis}) (i.e. increasing basis set size for fixed molecule size). This is because the dominant step of the NL calculations is mainly the double integral, which is not related to the basis set. The scalings of wall time with respect to the molecule size (M, the number of non-hydrogen atoms) in alanine poly-peptide systems are around $O(M^{3.0})$, $O(M^{3.44})$, and $O(M^{2.77})$ for F_{nuc}, G, and Hess respectively. They can be further

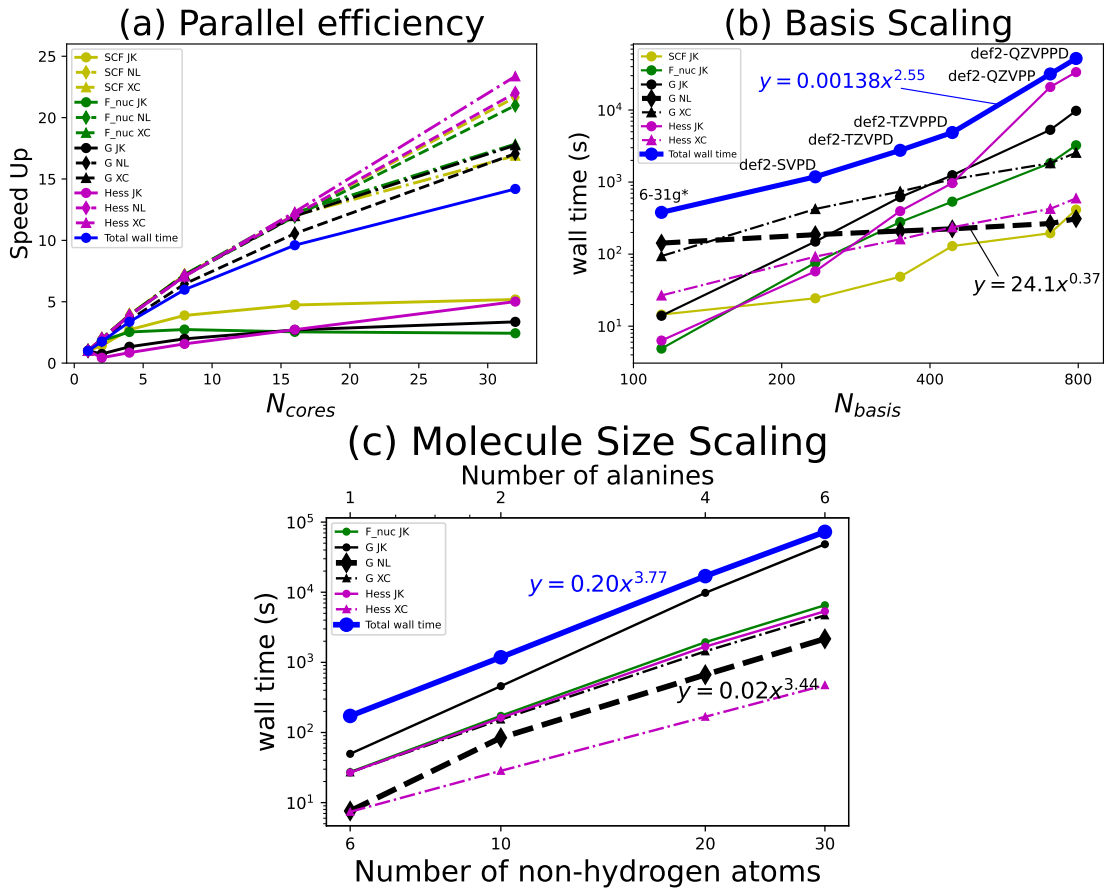

FIG. 1: Wall time for calculating the analytic frequencies with ωB97M-V under different conditions: (a) $(H_2O)_6$ using the def2-SVPD basis set as a function of the number of physical cores. (b) $(H_2O)_6$ system using different basis sets (6-31g*, def2-SVPD, def2-TZVPD, def2-TZVPPD, def2-QZVPP, def2-QZVPPD in order of increasing size), in calculations using 32 physical cores. (c) alanine polypeptide systems using the def2-SVPD basis set with 32 physical cores. We use benchmark-level accuracy for (a) and (b), with (99, 590)/SG-1 as the XC/NL grid type and 10^{-14} as the integral threshold, and routine production-level protocol for (c), with SG-2/SG-0 as the XC/NL grid type and 10^{-10} as the integral threshold.

reduced to $O(M^{2.84})$, $O(M^{2.90})$, and $O(M^{2.73})$ if only fitting the data with 20 and 30 non-hydrogen atoms, indicating the optimized code performs very well with the SG-0 grid.

IV. RESULTS AND DISCUSSION

A. Basis set and grid convergence

We explored the basis set and quadrature grid convergence of harmonic frequencies evaluated with B97M-V, ωB97X-V, and ωB97M-V functionals at their optimized geometries (OptGs) and compared them with B97-D and B3LYP-D3(BJ). These calculations used the (99, 590) XC integral grid, and the SG-1 NL grid. From Figure 2, it is evident that basis set convergence for water clusters is more difficult than for the HFREQ2014 set. The difference in root-mean-squared errors (RMSEs) obtained with def2-TZVP and def2-QZVPPD basis sets for the HFREQ2014 set is at most 4 cm^{-1}, around 10% of the method error. In contrast, the larger def2-TZVPPD basis is needed to achieve the same accuracy for the H2O set. As a result, we recommend def2-TZVP for common chemically-bonded systems and def2-TZVPPD for systems with noncovalent interactions such as water clusters.

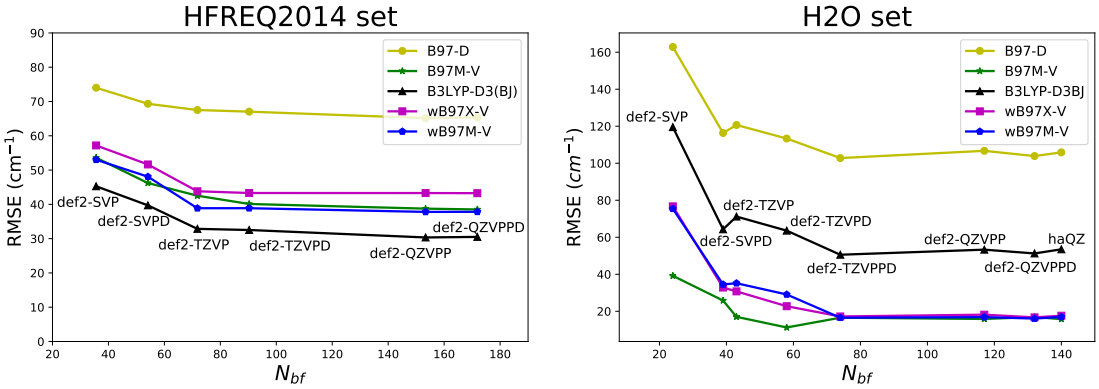

FIG. 2: Comparison of the RMSEs (cm^{-1}) of several basis sets relative to TBEs using the optimized geometries against their average number of basis functions (for the HFREQ2014 data set) or the number of functions on a single water molecule (for the H2O cluster data set) (N_{bf}) Tested basis sets include def2-SVP, def2-SVPD, def2-TZVP, def2-TZVPD, def2-TZVPPD, def2-QZVPP, def2-QZVPPD, and haQZ (only for the H2O set).

Figure 3 displays the RMSEs produced with different grids on the HFREQ2014 data set. It turns out that quadrature grid convergence is quite easy to achieve for simulating frequencies. If we regard 1 cm^{-1} of RMSE difference with the biggest tested grid as the accepted threshold, then SG-2 is large enough for semi-local XC integrals and SG-0 is large enough for the nonlocal (NL)

integrals of VV10. The smaller SG-1 grid for XC integration can also offer an RMSE difference of at most 4 cm^{-1}. Table II and Table S1.3 further validate this conclusion on the H2O set and the DiatomicU set. We only found that the XC part of B97M-V is a little more sensitive to the grid type, especially the pruning associated with the use of standard grids. For example, SG-3 is a pruned subset of (99, 590) grid and its performance is expected to be fairly similar to (99, 590) and better than (75, 302). However, the difference between RMSEs obtained with SG-3/SG-1 and (99, 590)/SG-1 on the H20 data set is 2.42 cm^{-1}, much bigger than the difference between (75, 302)/SG-1 and (99, 590)/SG-1 (0.66 cm^{-1}). One possible reason is that SG-3 removes some grid points far away from the nucleus, which are important to describe hydrogen bonds. From Table S1.3, we can see that the low frequencies (< 1000 cm^{-1}) are more affected than the high frequencies (≥ 1000 cm^{-1}). Therefore, we recommend the SG-2/SG-0 grid combination for common functionals on chemically-bonded systems and (75, 302)/SG-1 for sensitive functionals on hydrogen-bonding systems, provided that SCF and CPSCF can be converged. It's worth noting that purely dispersion-bound systems such as Ar_2 and He_2 may require a larger grid according to Ref 98. Additionally, some functionals, like SCAN, exhibit poor grid convergence behavior on all systems, as shown in Figure S18 of Ref 98. In fact, we also tested SCAN on the HFREQ2014 dataset using (99, 590) and (250, 974) grids, and the RMSE difference is as high as 8 cm^{-1}.

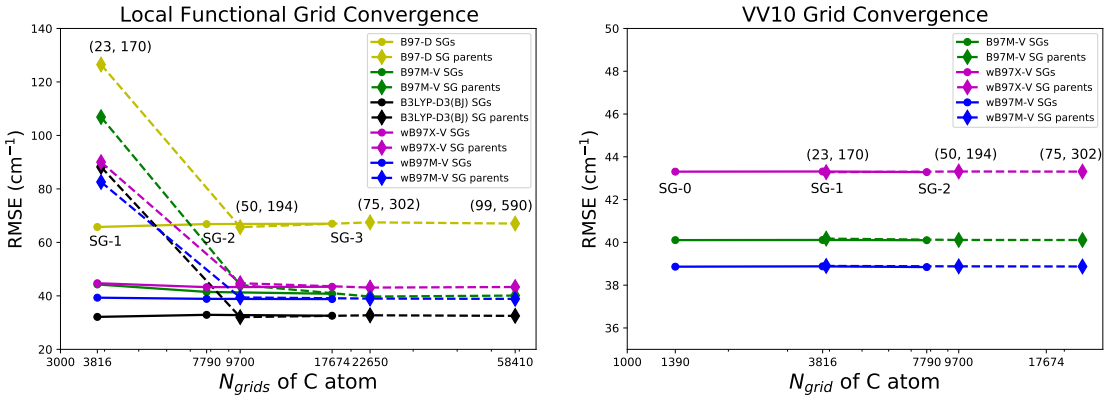

FIG. 3: Comparison of the RMSEs (cm^{-1}) of several grid types for XC and NL functionals relative to TBEs using the optimized geometries against the number of grid points for one carbon atom on the HFREQ2014 set. Tested grid types include the standard grids (SG-0/1/2/3) in Q-Chem and their parents [(23, 170), (50, 194), (75, 302), (99, 590)].

TABLE II: Comparison of the RMSEs (cm^{-1}) of several grid types for some representative functionals relative to TBEs using the optimized geometries on the H2O set. For B97-D and B3LYP-D3(BJ), only one entry is displayed at each XC grid level since they have no NL component.

XC/NL Grid Type	**B97-D**	**B97M-V**	**B3LYP**	**ωB97X-V**	**ωB97M-V**
SG-2/SG-0	112.72	16.92	63.31	22.72	29.31
SG-3/SG-0	113.19	13.71	63.71	22.72	29.48
SG-3/SG-1		13.67		22.70	29.22
(75, 302)/SG-1		11.91			
(99, 590)/SG-1	113.35	11.25	63.57	22.74	29.08
(99, 590)/(50,194)		11.26		22.75	29.08

B. Effect of VV10

Figure 4 compares the RMSEs of B97M-V, ωB97X-V, and ωB97M-V with VV10, without VV10, and with D3(BJ) [namely replacing VV10 with D3(BJ)]. The inclusion of the dispersion correction [both D3(BJ) and VV10] has a minimal impact on the Covalent Set and a slightly bigger impact on the Noncovalent Set. Therefore, the following analysis is based on the Noncovalent Set and should be suitable for molecules with non-covalent interactions. For B97M-V, both D3(BJ) and VV10 can lower the RMSEs of low frequencies and high frequencies, implying the importance of dispersion correction on a semi-local functional such as B97M-V. For ωB97X-V and ωB97M-V, the high-frequency RMSEs are increased with both D3(BJ) and VV10, while the low-frequency RMSEs are reduced with VV10. If we compare the RMSEs on each subset (Figure S1), we can see VV10 is able to improve the low-frequency predictions on all Noncovalent subsets, which is consistent with VV10's goal of better describing long-range correlation predictions, namely weak interactions. However, the consistent improvement is small and only exists at the optimized geometries in this work.

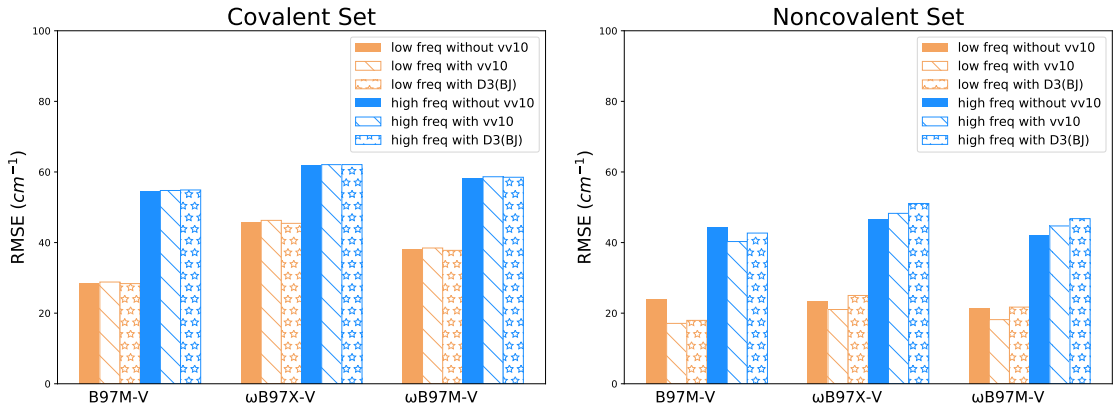

FIG. 4: Comparison of the RMSEs (cm^{-1}) of low frequencies (< 1000 cm^{-1}) and high frequencies (≥ 1000 cm^{-1}) of B97M-V, ωB97X-V, and ωB97M-V with VV10, without VV10, and with D3(BJ) [replacing VV10 with D3(BJ)] relative to TBEs at the optimized geometries on the Covalent set (with def2-TZVP for the HFREQ2014 subset and aug-cc-pwCVTZ for the Diatomic subsets) and Noncovalent Set (with aug-cc-pVTZ for the P subset, the def2-QZVPP for the H2O and V30 sets, aug-cc-pVQZ for the H2S set, and the def2-QZVPPD for the N2O and CO2 sets)

C. Comparison of functionals on all data sets

Figure 5 shows some recent or popular functionals' performance at theoretical best geometries (TBGs) and optimized geometries (OptGs). The SCF for M06-L cannot be converged for some radicals, and thus M06-L results for the Covalent Set are not presented. The D3(BJ) empirical correction is added to any functional without its own dispersion component.

The first striking outcome of Figure 5 is that the RMSEs of all functionals at TBGs are significantly lower than those at OptGs for predicting high frequencies. We tend to always perform frequency calculations at the optimized geometry because this is essential to reliably characterize stationary points and avoid imaginary frequencies. One might also believe that there exists cancellation of method error and geometry error at the optimized (i.e., equilibrium) geometry of the same-level method and thus frequency prediction could be more accurate. This is consistent with our results for low frequencies, especially on the Noncovalent Set, where a lot of imaginary frequencies appear at TBGs. However, this is clearly not true for simulating high frequencies. One possible explanation is that the high frequencies imply that the potential energy surface (PES) curve is steep and sensitive to even very small structure changes. Therefore, a better geometry

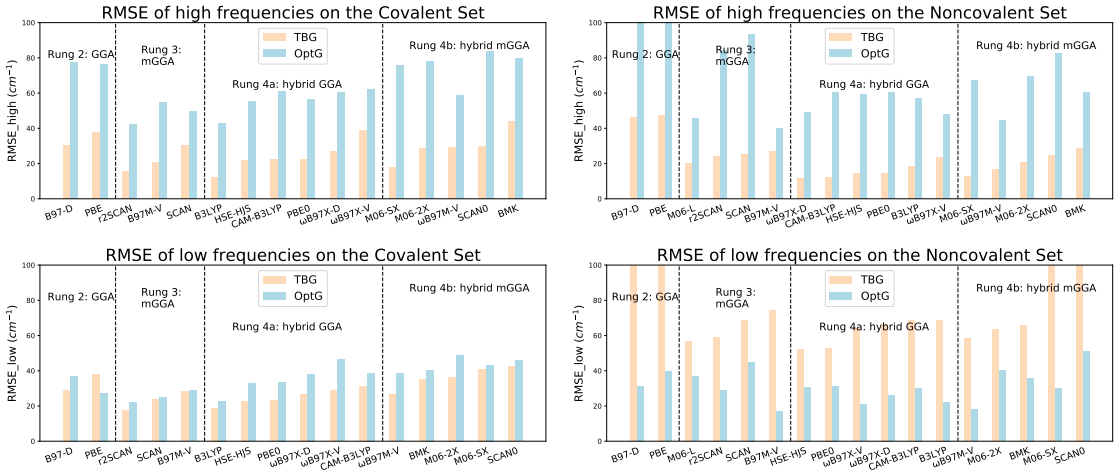

FIG. 5: Comparison of the RMSEs (cm^{-1}) of low frequencies (< 1000 cm^{-1}) and high frequencies (≥ 1000 cm^{-1}) of different functionals relative to TBEs using TBGs and optimized geometries (OptGs) on the Covalent Set and Noncovalent Set (with the same basis sets as Figure 4). The results are organized left to right in order of increasing RMSE using TBGs on each rung of Jacob's Ladder. The D3(BJ) empirical correction is added to any functional without its own dispersion component.

will improve frequency prediction. Given that geometry optimization consumes less computational resources than frequency calculations, it can therefore be useful to geometry optimize with a more accurate (and more expensive) method than that used for frequency evaluation when high frequencies (≥ 1000 cm^{-1}) are of primary interest.

Turning to the performance of individual functionals, the conclusions are very different for the Covalent Set and Noncovalent Set. It is evident from Figure 5 and Figure S2 that B3LYP offers the overall smallest RMSEs at TBGs and nearly the smallest RMSEs at OptGs on the Covalent Set. While we do notice a significant improvement of all mGGAs relative to GGAs (B97-D and PBE), Jacob's Ladder[99] is partially violated since the best hybrid mGGAs (ωB97M-V and M06-SX) are not better than the best hybrid GGA (B3LYP). In fact, r2SCAN, a semi-local mGGA, is the second-best functional at TBGs and can slightly outperform B3LYP at OptGs. It is possible that present functionals like B3LYP or r2SCAN might have reached the maximum capability of semi-local/hybrid DFT to predict the frequencies of common small molecules. It is also possible that the hybrid mGGAs can be further improved because of their enormous functional flexibility.[1]

The molecules included in the Covalent Set are too small for intramolecular dispersion to be significant, and therefore the effect of the VV10 component of the tested functionals is very small

as discussed in the previous subsection. However, the situation changes for the intermolecular interactions associated with the Noncovalent Set. Firstly, the inclusion of many low-frequency vibrations causes the overall RMSE at OptG to be smaller than the RMSE at TBG. Secondly, we observe dramatic improvements in frequency prediction in the VV10-containing functionals using OptGs. Figure 5 shows that B97M-V (overall RMSE of 29.4 cm^{-1}) dramatically outperforms r2SCAN (RMSE of 59.3 cm^{-1}) at the mGGA level and both ωB97M-V (RMSE of 32.3 cm^{-1}) and ωB97X-V (RMSE of 35.4 cm^{-1}) outperform B3LYP (RMSE of 41.0 cm^{-1}) significantly at the hybrid level. When we look at each subset separately in Figure S3, we can observe that the main advantage of the VV10-containing functionals comes from the H2O set. Figure S4 also shows that VV10-containing functionals describe dipole-dipole interactions better than pure dispersion. This is a surprising result that seems at odds with the design goal of using VV10 to better describe weak interactions, and could merit further studies, and/or support the idea of using (finite difference) frequency information in the development of future functionals.

D. Scaling Factors for New Developed Functionals

The data presented in previous sections are all based on the comparison of calculated harmonic frequencies and corresponding TBEs. However, in practice, many researchers prefer to employ scaled harmonic frequencies to approximate (anharmonic) experimental fundamental frequencies and to evaluate the zero-point vibrational energy (ZPVE). Therefore, we present the scaling factors and after-scaling RMSEs of some recent functionals (i.e., SCAN, r2SCAN, B97M-V, ωB97X-V, ωB97M-V, SCAN0, M06-SX, and HSE-HJS) with the def2-TZVP basis set in Table III. For a detailed error display, please see Table S1.6. The data set used here is from ref 56 and most TBGs are from the HFREQ2014 set. Only CH_3OH TBG is from CCCBDB, optimized by CCSD(T)/aug-cc-pVTZ, and unrestricted species TBGs are from the DiatomicU set.

As shown in Table III, RMSEs at TBGs are larger than those at OptGs for predicting fundamental frequencies but smaller for predicting ZPVEs. Although no modern functional can outperform B3LYP (RMSE of 19.44 cm^{-1} at OptGs), scaling significantly lowers functional sensitivity for fundamentals (the biggest RMSE at OptGs is just 28.3 cm^{-1} here). Similar findings hold true for ZPVEs, however, r2SCAN can provide RMSE that is comparable to B3LYP at TBGs and even smaller at OptGs. Compared with the result of ref 56, the optimal scaling factors of most functionals for fundamental frequencies and ZPVE are still around 0.96 and 0.98 respectively. Note

TABLE III: The scaling factors (λ) of some recent functionals with the def2-TZVP basis set for predicting fundamental frequencies and zero-point vibrational energy (ZPVE), and their RMSEs (cm^{-1} for frequency and kcal/mol for ZPVE) after scaling. The D3(BJ) empirical correction is added to any functional without its own dispersion component. Note that SCAN is tested at the same grid type (99,590) as other functionals rather than at its own converged grid type.

Property	**Result**		**SCAN**	**r2SCAN**	**B97M-V**	**ωB97X-V**	**SCAN0**	**M06-SX**	**HSE-HJS**	**ωB97M-V**	**B3LYP**
fundamental frequency	**TBG**	λ	0.962	0.962	0.963	0.952	0.954	0.959	0.957	0.959	0.964
		RMSE	30.9	28.4	28.1	30.7	35.6	31.2	32.4	28.5	25.6
	OptG	λ	0.963	0.967	0.957	0.954	0.941	0.949	0.958	0.958	0.967
		RMSE	27.6	21.5	27.8	25.4	25.3	28.3	25.5	24.5	19.4
ZPVE	**TBG**	λ	0.988	0.989	0.984	0.977	0.973	0.979	0.984	0.984	0.989
		RMSE	0.105	0.057	0.099	0.080	0.114	0.101	0.073	0.084	0.056
	OptG	λ	0.986	0.991	0.980	0.978	0.965	0.972	0.983	0.983	0.990
		RMSE	0.123	0.085	0.133	0.128	0.148	0.148	0.117	0.115	0.092

that the data set only involves small molecules here so it is not clear how well these conclusions will transfer to larger systems with significant noncovalent interactions.

V. CONCLUSIONS

In this work, we have formulated and efficiently implemented the analytical second derivatives of the nonlocal (NL) correlation functional, VV10. Tests of our OpenMP NL implementation establish that its parallel performance is quite good out to at least 32 cores. Furthermore, aside from the smallest basis sets, we have shown that the computational time for the NL part is negligible compared with that of the entire job.

As an application of the new analytical derivative code, we have also examined the performance of some recent or popular functionals for molecular vibrational frequencies. The assessment work builds on a number of previous efforts to establish benchmark data sets, which we have compiled into a Covalent Set and a Noncovalent Set. The Covalent Set contains small molecules without weak interactions while the Noncovalent Set can represent chemical systems containing weak intermolecular interactions. As shown in Table IV, our conclusions are different for these two kinds of systems. While VV10-containing functionals provide little or no advantage in the accuracy of

harmonic frequencies for small molecules, recent functionals such as B97M-V, ωB97X-V, and ωB97M-V provide very significant improvements for harmonic frequencies in polar molecular complexes. It is a fascinating question as to whether those same advantages will hold for vibrational frequencies in larger molecules. At the moment, a lack of suitable benchmarks for such molecules prevents an answer.

Finally, we also examined scaling factors for harmonic vibrational frequencies to permit direct comparison against (anharmonic) experimental fundamental vibrational frequencies and to evaluate the ZPVEs. B3LYP-D3(BJ) provides the smallest RMSE after scaling although the importance of functional choice is greatly reduced by scaling, at least for the small molecules which we have assessed.

TABLE IV: Broad conclusions and recommendations for simulating molecular harmonic frequencies (and ZPVE) for small molecules and weakly interacting systems. Note that choice of functional is less important if frequencies are scaled to compare against experiments, at least for small molecules.

Conclusions	Small molecules	Weak-interaction systems
Recommended basis set	def2-TZVP	def2-TZVPPD (or larger)
Recommended XC/NL grid	SG-2/SG-0	SG-2/SG-0 typically but (75, 302)/SG-1 for sensitive functionals
Effect of VV10	minimal	helpful for low-frequencies
Recommended functional	B3LYP-D3(BJ), r2SCAN-D3(BJ)	B97M-V, ωB97X-V, ωB97M-V

SUPPORTING INFORMATION

Additional figures (SI.pdf)

S1-data_analysis.xlsx

S2-raw_data.xlsx

AUTHOR DECLARATIONS

Martin Head-Gordon is a part-owner of Q-Chem, which is the software platform used to perform the developments and calculations described in this work. The other authors declare no competing financial interests.

ACKNOWLEDGMENTS

This work was supported by the Director, Office of Science, Office of Basic Energy Sciences, of the U.S. Department of Energy through the Gas Phase Chemical Physics Program, under Contract No. DE-AC02-05CH11231. Additional support to X.F. and M.H.-G. was provided through NIH grant R44GM121126-02. This research used computational resources of the National Energy Research Scientific Computing Center, a DOE Office of Science User Facility supported by the Office of Science of the U.S. Department of Energy under Contract No. DE-AC02-05CH11231.

REFERENCES

[1]N. Mardirossian and M. Head-Gordon, "Thirty years of density functional theory in computational chemistry: An overview and extensive assessment of 200 density functionals," Mol. Phys. **115**, 2315–2372 (2017).

[2]M. A. Palafox, "Dft computations on vibrational spectra: Scaling procedures to improve the wavenumbers," Physical Sciences Reviews **3**, 20170184 (2018).

[3]J. C. Zapata Trujillo and L. K. McKemmish, "Meta-analysis of uniform scaling factors for harmonic frequency calculations," WIREs Comput. Mol. Sci. **12**, e1584 (2021).

[4]J. Liang, X. Feng, D. Hait, and M. Head-Gordon, "Revisiting the performance of time-dependent density functional theory for electronic excitations: Assessment of 43 popular and recently developed functionals from rungs one to four," J. Chem. Theory Comput. (2022), 10.1021/acs.jctc.2c00160.

[5]S. Kristyán and P. Pulay, "Can (semi)local density functional theory account for the London dispersion forces?" Chem. Phys. Lett. **229**, 175–180 (1994).

[6]J. Pérez-Jordá and A. Becke, "A density-functional study of van der Waals forces: Rare gas diatomics," Chem. Phys. Lett. **233**, 134–137 (1995).

[7]P. Hobza, J. šponer, and T. Reschel, "Density functional theory and molecular clusters," J. Comput. Chem. **16**, 1315–1325 (1995).

[8]A. Najibi and L. Goerigk, "The nonlocal kernel in van der Waals density functionals as an additive correction: An extensive analysis with special emphasis on the b97m-v and ωb97m-v approaches," J. Chem. Theory Comput. **14**, 5725–5738 (2018).

[9]J. Klimeš and A. Michaelides, "Perspective: Advances and challenges in treating van der waals dispersion forces in density functional theory," J. Chem. Phys. **137**, 120901 (2012).

[10]M. Stöhr, T. Van Voorhis, and A. Tkatchenko, "Theory and practice of modeling van der waals interactions in electronic-structure calculations," Chem. Soc. Rev. **48**, 4118–4154 (2019).

[11]A. D. Becke and E. R. Johnson, "Exchange-hole dipole moment and the dispersion interaction revisited," J. Chem. Phys. **127**, 154108 (2007).

[12]A. Tkatchenko and M. Scheffler, "Accurate molecular van der waals interactions from ground-state electron density and free-atom reference data," Phys. Rev. Lett. **102**, 073005 (2009).

[13]S. Grimme, "Semiempirical gga-type density functional constructed with a long-range dispersion correction," J. Comput. Chem. **27**, 1787–1799 (2006).

[14]S. Grimme, J. Antony, S. Ehrlich, and H. Krieg, "A consistent and accurate ab initio parametrization of density functional dispersion correction (dft-d) for the 94 elements h-p," J. Chem. Phys. **132**, 154104 (2010).

[15]S. Grimme, S. Ehrlich, and L. Goerigk, "Effect of the damping function in dispersion corrected density functional theory," J. Comput. Chem. **32**, 1456–1465 (2011).

[16]S. Grimme, A. Hansen, J. G. Brandenburg, and C. Bannwarth, "Dispersion-corrected mean-field electronic structure methods," Chem. Rev. **116**, 5105–5154 (2016).

[17]H.-V. Nguyen and G. Galli, "A first-principles study of weakly bound molecules using exact exchange and the random phase approximation," J. Chem. Phys. **132**, 044109 (2010).

[18]W. Zhu, J. Toulouse, A. Savin, and J. G. Ángyán, "Range-separated density-functional theory with random phase approximation applied to noncovalent intermolecular interactions," J. Chem. Phys. **132**, 244108 (2010).

[19]G. P. Chen, V. K. Voora, M. M. Agee, S. G. Balasubramani, and F. Furche, "Random-phase approximation methods," Ann. Rev. Phys. Chem. **68**, 421–445 (2017).

[20]L. Goerigk and S. Grimme, "Double-hybrid density functionals," WIRes: Comput. Mol. Sci. **4**, 576–600 (2014).

[21]J. M. Martin and G. Santra, "Empirical double-hybrid density functional theory: A 'third way'in between wft and dft," Isr. J. Chem. **60**, 787–804 (2020).

[22]M. Dion, H. Rydberg, E. Schröder, D. C. Langreth, and B. I. Lundqvist, "Van der Waals density functional for general geometries," Phys. Rev. Lett. **92**, 246401 (2004).

[23]K. Lee, E. D. Murray, L. Kong, B. I. Lundqvist, and D. C. Langreth, "Higher-accuracy van der Waals density functional," Phys. Rev. B **82**, 081101 (2010).

[24]O. A. Vydrov and T. Van Voorhis, "Nonlocal van der Waals density functional made simple," Phys. Rev. Lett. **103**, 063004 (2009).

[25]O. A. Vydrov and T. Van Voorhis, "Nonlocal van der Waals density functional: The simpler the better," J. Chem. Phys. **133**, 244103 (2010).

[26]J. Calbo, E. Ortí, J. C. Sancho-García, and J. Aragó, "The nonlocal correlation density functional vv10: a successful attempt to accurately capture noncovalent interactions," in *Ann. Rep. Comput. Chem.*, Vol. 11 (Elsevier, 2015) pp. 37–102.

[27]N. Mardirossian and M. Head-Gordon, "ωb97x-v: A 10-parameter, range-separated hybrid, generalized gradient approximation density functional with nonlocal correlation, designed by a survival-of-the-fittest strategy," Phys. Chem. Chem. Phys. **16**, 9904 (2014).

[28]N. Mardirossian and M. Head-Gordon, "Mapping the genome of meta-generalized gradient approximation density functionals: The search for b97m-v," J. Chem. Phys. **142**, 074111 (2015).

[29]N. Mardirossian and M. Head-Gordon, "ωb97m-v: A combinatorially optimized, range-separated hybrid, meta-gga density functional with vv10 nonlocal correlation," J. Chem. Phys. **144**, 214110 (2016).

[30]R. Sabatini, T. Gorni, and S. De Gironcoli, "Nonlocal van der waals density functional made simple and efficient," Phys. Rev. B **87**, 041108 (2013).

[31]P. Pulay, "Analytical derivative methods in quantum chemistry," Adv. Chem. Phys. **67**, 241–286 (1987).

[32]R. D. Amos and J. E. Rice, "Implementation of analytic derivative methods in quantum chemistry," Comput. Phys. Rep. **10**, 147–187 (1989).

[33]J. Pople, R. Krishnan, H. Schlegel, and J. S. Binkley, "Derivative studies in hartree-fock and møller-plesset theories," Int. J. Quantum Chem. **16**, 225–241 (1979).

[34]M. Frisch, M. Head-Gordon, and J. Pople, "Direct analytic scf second derivatives and electric field properties," Chem. Phys. **141**, 189–196 (1990).

[35]B. G. Johnson and M. J. Fisch, "An implementation of analytic second derivatives of the gradient-corrected density functional energy," J. Chem. Phys. **100**, 7429–7442 (1994).

[36]P. Deglmann, F. Furche, and R. Ahlrichs, "An efficient implementation of second analytical derivatives for density functional methods," Chem. Phys. Lett. **362**, 511–518 (2002).

[37]S. K. Wolff, "Analytical second derivatives in the amsterdam density functional package," Int. J. Quantum Chem. **104**, 645–659 (2005).

[38]D. Bykov, T. Petrenko, R. Izsák, S. Kossmann, U. Becker, E. Valeev, and F. Neese, "Efficient implementation of the analytic second derivatives of hartree–fock and hybrid dft energies: a detailed analysis of different approximations," Mol. Phys. **113**, 1961–1977 (2015).

[39]R. I. Delgado-Venegas, D. Mejía-Rodríguez, R. Flores-Moreno, P. Calaminici, and A. M. Köster, "Analytic second derivatives from auxiliary density perturbation theory," J. Chem. Phys. **145**, 224103 (2016).

[40]Y. Gu, Z. Zhu, and X. Xu, "Second-order analytic derivatives for xyg3 type of doubly hybrid density functionals: theory, implementation, and application to harmonic and anharmonic vibrational frequency calculations," J. Chem. Theory Comput. **17**, 4860–4871 (2021).

[41]A. S. Abbott, B. Z. Abbott, J. M. Turney, and H. F. Schaefer III, "Arbitrary-order derivatives of quantum chemical methods via automatic differentiation," J. Phys. Chem. Lett. **12**, 3232–3239

(2021).

[42]M. F. Kasim, S. Lehtola, and S. M. Vinko, "Dqc: A python program package for differentiable quantum chemistry," J. Chem. Phys. **156**, 084801 (2022).

[43]P. Sałek and A. Hesselmann, "A self-contained and portable density functional theory library for use in ab initio quantum chemistry programs," Journal of computational chemistry **28**, 2569–2575 (2007).

[44]G. Mazur, M. Makowski, R. Łazarski, R. Włodarczyk, E. Czajkowska, and M. Glanowski, "Automatic code generation for quantum chemistry applications," International Journal of Quantum Chemistry **116**, 1370–1381 (2016).

[45]H. J. van Dam, "A comparison of different methods to implement higher order derivatives of density functionals," Tech. Rep. (Brookhaven National Lab.(BNL), Upton, NY (United States), 2016).

[46]S. Lehtola, C. Steigemann, M. J. Oliveira, and M. A. Marques, "Recent developments in libxc—a comprehensive library of functionals for density functional theory," SoftwareX **7**, 1–5 (2018).

[47]R. Sabatini, E. Küçükbenli, C. H. Pham, and S. de Gironcoli, "Phonons in nonlocal van der Waals density functional theory," Phys. Rev. B **93**, 235120 (2016).

[48]K. Miwa, "Linear response calculation with nonlocal van der Waals density functionals," Phys. Rev. B **105**, 024109 (2022).

[49]K.-Y. Liu, J. Liu, and J. M. Herbert, "Accuracy of finite-difference harmonic frequencies in density functional theory," J. Comput. Chem. **38**, 1678–1684 (2017).

[50]S. M. Sharada, D. Stück, E. J. Sundstrom, A. T. Bell, and M. Head-Gordon, "Wavefunction stability analysis without analytical electronic hessians: Application to orbital-optimised second-order Møller–Plesset theory and vv10-containing density functionals," Mol. Phys. **113**, 1802–1808 (2015).

[51]J. A. Pople, H. B. Schlegel, R. Krishnan, D. J. Defrees, J. S. Binkley, M. J. Frisch, R. A. Whiteside, R. F. Hout, and W. J. Hehre, "Molecular orbital studies of vibrational frequencies," Int. J. Quantum Chem. **20**, 269–278 (2009).

[52]J. P. Merrick, D. Moran, and L. Radom, "An evaluation of harmonic vibrational frequency scale factors," J. Phys. Chem. A **111**, 11683–11700 (2007).

[53]I. M. Alecu, J. Zheng, Y. Zhao, and D. G. Truhlar, "Computational thermochemistry: Scale factor databases and scale factors for vibrational frequencies obtained from electronic model

chemistries," J. Chem. Theory Comput. **6**, 2872–2887 (2010).

[54]M. Biczysko, P. Panek, G. Scalmani, J. Bloino, and V. Barone, "Harmonic and anharmonic vibrational frequency calculations with the double-hybrid B2PLYP method: Analytic second derivatives and benchmark studies," J. Chem. Theory Comput. **6**, 2115–2125 (2010).

[55]M. L. Laury, M. J. Carlson, and A. K. Wilson, "Vibrational frequency scale factors for density functional theory and the polarization consistent basis sets," J. Comput. Chem. **33**, 2380–2387 (2012).

[56]M. K. Kesharwani, B. Brauer, and J. M. L. Martin, "Frequency and zero-point vibrational energy scale factors for double-hybrid density functionals (and other selected methods): Can anharmonic force fields be avoided?" J. Phys. Chem. A **119**, 1701–1714 (2014).

[57]B. Chan and L. Radom, "Frequency scale factors for some double-hybrid density functional theory procedures: Accurate thermochemical components for high-level composite protocols," J. Chem. Theory Comput. **12**, 3774–3780 (2016).

[58]M. Katari, E. Nicol, V. Steinmetz, G. van der Rest, D. Carmichael, and G. Frison, "Improved infrared spectra prediction by DFT from a new experimental database," Chem. Eur. J. **23**, 8414–8423 (2017).

[59]D. O. Kashinski, G. M. Chase, R. G. Nelson, O. E. Di Nallo, A. N. Scales, D. L. VanderLey, and E. F. C. Byrd, "Harmonic vibrational frequencies: Approximate global scaling factors for TPSS, m06, and m11 functional families using several common basis sets," J. Phys. Chem. A **121**, 2265–2273 (2017).

[60]M. W. D. Hanson-Heine, "Benchmarking dft-d dispersion corrections for anharmonic vibrational frequencies and harmonic scaling factors," J. Phys. Chem. A **123**, 9800–9808 (2019).

[61]J. C. Zapata Trujillo and L. K. McKemmish, "Vibfreq1295: A new database for vibrational frequency calculations," J. Phys. Chem. A **126**, 4100–4122 (2022).

[62]Y. Ünal, W. Nassif, B. C. Özaydin, and K. Sayin, "Scale factor database for the vibration frequencies calculated in m06-2x, one of the DFT methods," Vib. Spectrosc. **112**, 103189 (2021).

[63]J. C. Zapata Trujillo and L. K. McKemmish, "Model chemistry recommendations for scaled harmonic frequency calculations: A benchmark study," The Journal of Physical Chemistry A (2023).

[64]L. Ravichandran and S. Banik, "Performance of different density functionals for the calculation of vibrational frequencies with vibrational coupled cluster method in bosonic representation," Theor. Chem. Acc. **137**, 1–14 (2017).

[65]J. C. Howard, J. D. Enyard, and G. S. Tschumper, "Assessing the accuracy of some popular DFT methods for computing harmonic vibrational frequencies of water clusters," J. Chem. Phys. **143**, 214103 (2015).

[66]A. D. Becke, "A multicenter numerical integration scheme for polyatomic molecules," J. Chem. Phys. **88**, 2547–2553 (1988).

[67]J. P. Perdew, K. Burke, and M. Ernzerhof, "Generalized gradient approximation made simple," Phys. Rev. Lett. **77**, 3865 (1996).

[68]J. Sun, A. Ruzsinszky, and J. P. Perdew, "Strongly constrained and appropriately normed semilocal density functional," Phys. Rev. Lett. **115**, 036402 (2015).

[69]J. W. Furness, A. D. Kaplan, J. Ning, J. P. Perdew, and J. Sun, "Accurate and numerically efficient r2scan meta-generalized gradient approximation," J. Phys. Chem. Lett. **11**, 8208–8215 (2020).

[70]Y. Zhao and D. G. Truhlar, "A new local density functional for main-group thermochemistry, transition metal bonding, thermochemical kinetics, and noncovalent interactions," J. Chem. Phys. **125**, 194101 (2006).

[71]J.-D. Chai and M. Head-Gordon, "Long-range corrected hybrid density functionals with damped atom–atom dispersion corrections," Phys. Chem. Chem. Phys. **10**, 6615 (2008).

[72]T. Yanai, D. P. Tew, and N. C. Handy, "A new hybrid exchange–correlation functional using the coulomb-attenuating method (cam-b3lyp)," Chem. Phys. Lett. **393**, 51–57 (2004).

[73]T. M. Henderson, B. G. Janesko, and G. E. Scuseria, "Generalized gradient approximation model exchange holes for range-separated hybrids," J. Chem. Phys. **128**, 194105 (2008).

[74]A. V. Krukau, O. A. Vydrov, A. F. Izmaylov, and G. E. Scuseria, "Influence of the exchange screening parameter on the performance of screened hybrid functionals," J. Chem. Phys. **125**, 224106 (2006).

[75]A. D. Becke, "Density-functional thermochemistry. iii. the role of exact exchange," J. Chem. Phys. **98**, 5648–5652 (1993).

[76]P. J. Stephens, F. J. Devlin, C. F. Chabalowski, and M. J. Frisch, "Ab initio calculation of vibrational absorption and circular dichroism spectra using density functional force fields," J. Phys. Chem. **98**, 11623–11627 (1994).

[77]A. D. Boese and J. M. L. Martin, "Development of density functionals for thermochemical kinetics," J. Chem. Phys. **121**, 3405–3416 (2004).

[78]Y. Wang, P. Verma, L. Zhang, Y. Li, Z. Liu, D. G. Truhlar, and X. He, "M06-sx screened-exchange density functional for chemistry and solid-state physics," Proc. Natl. Acad. Sci. U. S. A. **117**, 2294–2301 (2020).

[79]Y. Zhao and D. G. Truhlar, "The m06 suite of density functionals for main group thermochemistry, thermochemical kinetics, noncovalent interactions, excited states, and transition elements: Two new functionals and systematic testing of four m06-class functionals and 12 other functionals," Theor. Chem. Account **120**, 215–241 (2007).

[80]K. Hui and J.-D. Chai, "Scan-based hybrid and double-hybrid density functionals from models without fitted parameters," J. Chem. Phys. **144**, 044114 (2016).

[81]J. M. L. Martin and M. K. Kesharwani, "Assessment of ccsd(t)-f12 approximations and basis sets for harmonic vibrational frequencies," J. Chem. Theory Comput. **10**, 2085–2090 (2014).

[82]L. W. Bertels, J. Lee, and M. Head-Gordon, "Polishing the gold standard: The role of orbital choice in CCSD(T) vibrational frequency prediction," J. Chem. Theory Comput. **17**, 742–755 (2021).

[83]J. Lee and M. Head-Gordon, "Regularized orbital-optimized second-order møller–plesset perturbation theory: A reliable fifth-order-scaling electron correlation model with orbital energy dependent regularizers," J. Chem. Theory Comput. **14**, 5203–5219 (2018).

[84]K. A. Peterson and T. H. Dunning, "Accurate correlation consistent basis sets for molecular core–valence correlation effects: The second row atoms Al–Ar, and the first row atoms B–Ne revisited," J. Chem. Phys. **117**, 10548–10560 (2002).

[85]B. P. Prascher, D. E. Woon, K. A. Peterson, T. H. Dunning, and A. K. Wilson, "Gaussian basis sets for use in correlated molecular calculations. VII. valence, core-valence, and scalar relativistic basis sets for li, be, na, and mg," Theor. Chem. Acc. **128**, 69–82 (2010).

[86]J. C. Howard and G. S. Tschumper, "Benchmark structures and harmonic vibrational frequencies near the ccsd (t) complete basis set limit for small water clusters:(h2o) n= 2, 3, 4, 5, 6," J. Chem. Theory Comput. **11**, 2126–2136 (2015).

[87]J. C. Howard and G. S. Tschumper, "N-body: Many-body qm: Qm vibrational frequencies: Application to small hydrogen-bonded clusters," J. Chem. Phys. **139**, 184113 (2013).

[88]J. Hoja and A. D. Boese, "The v30 benchmark set for anharmonic vibrational frequencies of molecular dimers," arXiv preprint, arXiv:2209.04392 (2022).

[89]K. H. Lemke, "Structure and binding energy of the h2s dimer at the ccsd (t) complete basis set limit," J. Chem. Phys. **146**, 234301 (2017).

[90]S. R. Salmon, K. M. de Lange, and J. R. Lane, "Structure and abundance of nitrous oxide complexes in earth's atmosphere," J. Phys. Chem. A **120**, 2096–2105 (2016).

[91]K. M. de Lange and J. R. Lane, "Explicit correlation and intermolecular interactions: Investigating carbon dioxide complexes with the ccsd (t)-f12 method," J. Chem. Phys. **134**, 034301 (2011).

[92]E. Van Dornshuld and G. S. Tschumper, "Big changes for small noncovalent dimers: Revisiting the potential energy surfaces of (p2) 2 and (pccp) 2 with ccsd (t) optimizations and vibrational frequencies," J. Chem. Theory Comput. **12**, 1534–1541 (2016).

[93]E. Epifanovsky, A. T. Gilbert, X. Feng, J. Lee, Y. Mao, *et al.*, "Software for the frontiers of quantum chemistry: An overview of developments in the q-chem 5 package," J. Chem. Phys. **155**, 084801 (2021).

[94]F. Weigend and R. Ahlrichs, "Balanced basis sets of split valence, triple zeta valence and quadruple zeta valence quality for h to rn: Design and assessment of accuracy," Phys. Chem. Chem. Phys. **7**, 3297 (2005).

[95]D. Rappoport and F. Furche, "Property-optimized Gaussian basis sets for molecular response calculations," J. Chem. Phys. **133**, 134105 (2010).

[96]P. M. Gill, B. G. Johnson, and J. A. Pople, "A standard grid for density functional calculations," Chem. Phys. Lett. **209**, 506–512 (1993).

[97]S. Dasgupta and J. M. Herbert, "Standard grids for high-precision integration of modern density functionals: Sg-2 and SG-3," J. Comput. Chem. **38**, 869–882 (2017).

[98]S. P. Sitkiewicz, R. Zaleśny, E. Ramos-Cordoba, J. M. Luis, and E. Matito, "How reliable are modern density functional approximations to simulate vibrational spectroscopies?" J. Phys. Chem. Lett. **13**, 5963–5968 (2022).

[99]J. P. Perdew, A. Ruzsinszky, J. Tao, V. N. Staroverov, G. E. Scuseria, and G. I. Csonka, "Prescription for the design and selection of density functional approximations: More constraint satisfaction with fewer fits," J. Chem. Phys. **123**, 062201 (2005).